

Countergradient heat flux observations during the evening transition period

E. Blay–Carreras¹, E. R. Pardyjak², D. Pino^{1,3}, D. C. Alexander², F. Lohou⁴, and M. Lothon⁴

¹Department of Applied Physics, Universitat Politècnica de Catalunya · BarcelonaTech, Barcelona, Spain

²Department of Mechanical Engineering, University of Utah, Salt Lake City, UT USA

³Institute of Space Studies of Catalonia (IEEC–UPC), Barcelona, Spain

⁴Université de Toulouse/CNRS 5560, Laboratoire d’Aérodynamique, Toulouse, France

Correspondence to: E. Blay–Carreras (estel.blay@upc.edu)

Abstract. Gradient-based turbulence models generally assume that the buoyancy flux ceases to introduce heat into the surface layer of the atmospheric boundary layer in temporal consonance with the gradient of the local virtual potential temperature. Here, we hypothesize that during the evening transition a delay exists between the instant when the buoyancy flux goes to zero and the time when the local gradient of the virtual potential temperature indicates a sign change. This phenomenon is studied using a range of data collected over several Intensive Observational Periods (IOPs) during the Boundary Layer Late Afternoon and Sunset Turbulence field campaign conducted in Lannemezan, France. The focus is mainly on the lower part of the surface layer using a tower instrumented with high-speed temperature and velocity sensors.

The results from this work confirm and quantify a flux-gradient delay. Specifically, the observed values of the delay are ~ 30 to 80 min. The existence of the delay and its duration can be explained by considering the convective time scale and the competition of forces associated with the classical Rayleigh–Bénard problem. This combined theory predicts that the last eddy formed while the sensible heat flux changes sign during the evening transition should produce a delay. It appears that this last eddy is decelerated through the action of turbulent momentum and thermal diffusivities, and that the delay is related to the convective turn—over time—scale. Observations indicate that as horizontal shear becomes more important, the delay time apparently increases to values greater than the convective turnover time-scale.

1 Introduction

The general behavior of the diurnal cycle of the atmospheric boundary layer (ABL) under clear sky fair weather conditions is well-known (Stull, 1988). During the day, a convective boundary layer driven by surface and entrainment fluxes exists (Moeng and Sullivan, 1994; Sorbján, 1996; Sullivan et al., 1998; Pino et al., 2003; Fedorovich et al., 2001). Late in the afternoon, due to radiative cooling of the ground, a stable boundary layer (SBL), where turbulence may be suppressed, is created adjacent to the earth’s surface (Nieuwstadt, 1984; Mahrt, 1998; Beare et al., 2006). A residual layer (RL) of weak turbulence exists above this SBL. The RL occupies a similar space as the mixed layer of that day’s convective boundary layer (CBL). However, the details of certain processes, particularly those associated with non-stationary transitional periods are not as well understood. The transition occurring after the peak in solar insolation can be divided into two distinct periods: the *afternoon transition*, when the surface sensible heat flux starts to decrease from its midday maximum, and the *evening transition*, when the surface sensible heat flux becomes negative (Nadeau et al., 2011).

This paper focuses on the behavior of the buoyancy flux and temperature gradient in the surface layer during the evening transition period by analyzing measurements obtained during the Boundary Layer Late Afternoon and Sunset Turbulence (BLLAST, Lothon et al. (2014)) field campaign. BLLAST was conceived to study the late afternoon transition (LAT) processes in the ABL. Objectives of the BLLAST project include gaining a better understanding of (a) the importance of surface heterogeneity on the LAT and (b) the structure and evolution of the boundary layer itself during this period of the day. The team members of this

project include an international group of scientists from different countries in Europe and the USA. The main hypotheses to be tested during this study are focused on the afternoon transition; therefore, the observations obtained from BLLAST campaign provide a valuable framework to develop the present work.

In this work, we hypothesize that during the evening transition, a delay exists between the instant when the buoyancy flux goes to zero and the time when the local gradient of the virtual potential temperature indicates a sign change. While this hypothesis has received little attention during the transition period, Ghan (1981) and Franchitto and Rao (2003) attempted to find a relationship between the temperature gradient and the heat flux, considering the complete diurnal cycle. In addition, nonlocal modelling studies have been used to develop different theories about eddy diffusivity and countergradient transport (Deardorff, 1972; Holtslag and Moeng, 1991). Holtslag and Boville (1993) introduced a nonlocal term in the parameterization of vertical diffusion in the atmospheric boundary layer to account for convective situations where the heat flux can be counter to the local potential temperature gradient (positive heat flux and positive gradient of potential temperature). In this case, turbulence results from nonlocal transport, by eddies on the order of the size of the boundary layer. This mainly occurs at the upper part of the boundary layer, just below the entrainment zone and far from the surface layer.

Investigations using observations (Grimsdell and Angevine, 2002) or large-eddy simulations (Nieuwstadt and Brost, 1986; Sorbjan, 1997; Pino et al., 2006) have shown that entrainment fluxes introduce heat in the boundary layer after the sensible heat flux becomes negative, producing turbulence in the middle of the mixed layer several hours after sunset (demixing process). However, Darbieu et al. (2014) have recently shown, using LES and aircraft observations during the afternoon transition, that turbulence (TKE and variances) decreases earlier in the upper levels of the boundary layer. If this result is also true during the evening transition, it seems that demixing, if it exists, cannot also be attributed to entrainment. Again, none of these studies focused on the response of the surface layer during this transition.

At the surface layer, it is normally assumed that the buoyancy flux ceases to introduce heat into the ABL at the same instant that the gradient of the virtual potential temperature reflects this phenomenon. Most simulation models work using this basic concept. A good knowledge of the phenomenon and evolution of the afternoon/evening transition is crucial for developing more realistic models and creating better approximations (Sorbjan, 1997; Cole and Fernando, 1998; Edwards et al., 2006; Pino et al., 2006; Angevine, 2007; Nadeau et al., 2011).

The objective of this article is to investigate this phenomenon using a range of data collected over several days, focusing mainly on the lower surface layer, using a tower in-

strumented with fast response fine-wire (FW) thermocouples and sonic anemometers thermometers (SATs). Moreover, the hypothesis will be supported by theories that can explain this phenomenon, such as the inverse Bénard problem, the effect of convective time or the definition of convection characteristics with the help of the Monin–Obukhov length scale.

The paper is structured as follows. In Section 2, we present the theory supporting the main hypothesis of the article. In Section 3, we describe the BLLAST field campaign and the instruments selected to test the hypothesis including the method for identifying time periods of interest for the analysis. In Section 4, we present the results focusing on the delay and convective time analysis, the Monin–Obukhov length scale analysis and turbulent Rayleigh number analysis. Finally, Section 5 summarizes the results.

2 Background theory

The hypothesis, which was described in the introduction, can be related to the well-known Rayleigh–Bénard (R–B) problem (thermal instability) associated with the heating of a quiescent layer of fluid from below which ultimately results in turbulent free convection (Kundu and Cohen, 2010). The standard R–B problem is based on the idea that there is a layer of fluid heated from below, however, the upper part of the layer is heavy enough to stifle the convective movements. Both viscosity and thermal diffusivity make it difficult for convection movements to happen. Therefore, large temperature gradients are required to create the instability that makes movement possible. Here we consider similar physics, but in the opposite sense because during LAT the CBL is cooled from below. The idea was previously introduced and experimentally studied by Cole and Fernando (1998) who designed a laboratory water tank experiment to observe the decay of temperature and velocity fluctuations in the CBL in response to cooling the surface.

In both the classical R–B problem and the phenomena studied in this paper, a delay exists that is related with the buoyancy flux at the surface and convective movements. When the buoyancy flux ceases, the convective movements continue for some time. This delay can be similarly produced from the same factors that drive the classical R–B problem. In other words, the viscosity and the thermal diffusivity make it possible for this transition to happen in a more smooth way. The dimensionless parameter, which compares the destabilizing forces (buoyancy forces) with the stabilizing forces (viscosity and thermal diffusivity) is the Rayleigh number,

$$Ra = \frac{g\Delta\bar{\theta}_v(\Delta z)^3}{\theta_v\kappa\nu}, \quad (1)$$

where g is the gravitational constant, $\Delta\bar{\theta}_v$ is the average virtual potential temperature difference over the layer depth Δz (taken here as the height of the atmospheric near-surface

layer), κ is the molecular thermal diffusivity and ν is the molecular kinematic viscosity. For the classical R–B problem with heating from below, when the Rayleigh number reaches a critical value, Ra_{cr} , convective movement will start. In this paper, we provide preliminary evidence for a transitional turbulent Rayleigh number at which convective motions cease.

3 Methodology

This study was performed within the framework of the BLLAST field campaign. Amongst the wide range of instruments deployed during the campaign, a relatively short (10 m), but highly instrumented tower was selected to be used in this study. This tower, located at $43^\circ 07' 39.3''$ N and $00^\circ 21' 57.9''$ E, was selected because it was equipped with a large number of closely spaced sensors, and was placed over relatively simple and homogeneous terrain (flat grass field). The sensors deployed on the tower included SATs and FWs. The instrument–deployment strategy focused many sensors close to the ground in order to observe small and fast changes connected to this zone. Figure 1a shows the vertical location of the instruments on the 10–m mast and Fig. 1b shows an aerial view of the site where the tower was located.

Four Campbell Scientific sonic anemometer thermometers (CSAT3, Logan, UT) fit with $12.7\text{-}\mu\text{m}$ diameter Campbell Scientific E-TYPE model FW05 fine-wire thermocouples were mounted at the following heights: 2.23, 3.23, 5.27 and 8.22 m above ground. Closer to the ground, there were four additional FW05 sensors mounted at 0.091, 0.131, 0.191, and 0.569 m above ground. These small diameter thermocouples were selected to minimize solar loading and response time to turbulent temperature fluctuations. The lowest sensor was placed just in the grass canopy. The grass around this sensor was regularly trimmed to maintain a canopy height of approximately 7–9 cm. During the intensive observation periods (IOPs) the lowest FWs were installed during the afternoon through the entire transition period to provide an expanded dataset. All instruments recorded data at 20 Hz. However, 5–min block-averaged data are presented in the analysis shown below. All data were processed using the software package *EC-pack* (Van Dijk et al., 1998).

This study focuses on the analysis of the following group of IOP days during the BLLAST campaign: 24, 25, 27, 30 June and 1, 2 July 2011. These IOPs represent days when the 10–m tower was completely instrumented. Table 1 summarizes the information used to characterize the IOPs including the daily maximum surface sensible heat flux, the duration of the diurnal cycle and the days from the last rainfall.

The primary goal of this work is to characterize and understand the observed time delay between the instant when the buoyancy flux is zero and when the virtual potential temperature gradient changes sign. To sketch the change of sign of the gradient of virtual potential temperature, Fig. 2 shows the temporal evolution of the vertical profile of potential temper-

ature measured by the FWs located at the 10–m mast during the evening on 1 July 2011. We can observe how, at the lowest levels, the gradient of potential temperature changes sign from negative to positive.

The instrumentation used in the campaign included fewer SATs than FW thermocouples, so the instruments were not always collocated. However, to include the effects of humidity, we use the measurements made by the SATs located at 2.23 and 3.23 m because these are the lowest sensors which can be used to simultaneously measure virtual potential temperature gradients and buoyancy flux.

To estimate the virtual potential temperature (θ_v), we assumed that the virtual temperature (T_v) can be approximated by the sonic temperature. The virtual potential temperature was then estimated using the adiabatic lapse rate (Γ) as follows: $\theta_v = T_v + \Gamma z$. Gradients were then computed using finite differences (Chapra and Canale, 1998).

The following paragraphs describe how this delay is determined. Figure 3 shows the observed temporal evolution of θ_v at 2.23 and 3.23 m during two IOP and illustrates the time when the change in sign of the gradient between the virtual potential temperature at the two levels occurs. The change in sign of the gradient first occurs at 1836 UTC for the 30 June 2011 and at 1851 UTC on 1 July 2011. The buoyancy flux was computed using:

$$BF = \frac{g}{T_v} \overline{w'\theta'_v}. \quad (2)$$

Here, $\overline{w'\theta'_v}$ is the vertical kinematic flux of virtual potential temperature. The lowest sensor (2.23 m) is used to define when the buoyancy flux ceases. In other words, when there is no more heat coming from the ground being measured at that probe. For instance, on 30 June and on 1 July 2011 the lower sensor shows that the flux ceases at approximately 1818 UTC and 1754 UTC, respectively. The delay time between when temperature gradient and buoyancy flux pass through zero is then simply the difference between the two times.

To develop the theory for the inverse R–B problem, the area selected is the lowest surface layer specifically from 2.23 to 8.2 m, which is the area with an evolution closer to the idea proposed by Bénard. First, we calculate the turbulent thermal diffusivity (K_H) and the turbulent viscosity (K_M). These two parameters can be estimated using the following equations.

$$K_H = \overline{w'\theta'_v} / \frac{\partial \overline{\theta}_v}{\partial z}, \quad (3)$$

$$K_M = -u_*^2 / \frac{\partial S}{\partial z}, \quad (4)$$

where u_* is the friction velocity and S is the mean wind speed. There is relatively little variability in these parameters during the day, therefore they are estimated by using the maximum buoyancy flux to avoid possible influences of the

skin flow close to the afternoon transition and to be consistent during all IOPs.

4 Results and discussion

4.1 Delay time analysis

Using the procedure described above, the delay time (DT) was computed for all IOPs. The results for all the studied IOPs are summarized in Fig. 4, where the instants when the buoyancy flux and the virtual potential temperature gradient change sign are shown. As is shown in the figure, this delay was present on all days analyzed. The delay varies from around 30 to 80 min. The numerical values for the delay time for all IOPs are given in Table 1.

A possible explanation for the occurrence of this delay can be related to eddy movements associated with warm air plumes that form at the surface. The moment that the buoyancy flux transitions from positive to negative values indicates that no more heat is being introduced to the atmosphere from the ground. Additionally, the upward movement due to warming of the air next to the ground (formation of new thermal plumes) also stops. However, these movements are not instantaneous movements. Quite the opposite, these movements start at the ground, mix through the surface layer and potentially move upward, crossing the entire boundary layer up to the entrainment zone and then descend with the warm air introduced by the overshoots of the eddies in the free atmosphere (i.e., the movements act over an eddy turnover period of time). When the introduction of heat stops ($BF = 0 \text{ W m}^{-2}$), the last eddy forms and continues to move through the boundary layer. During this eddy turnover time period, the surface layer cools, changing the sign of the temperature gradient. Consequently, the surface layer does not instantaneously respond when the surface flux stops, because the mixing (and heat transfer) continues during one eddy turnover time. This idea has been presented in different studies, for instance by (Sorbjan, 1997), although it focuses mainly on movements in the entrainment zone and not at the ground. Further, this hypothesis also is compatible with the existence of a neutral layer above the decoupled stable surface layer, where, due to entrainment, turbulence may still exist (Nieuwstadt and Brost, 1986; Grimsdell and Angevine, 2002; Pino et al., 2006).

An analysis of the dimensionless temperature gradient (ϕ_h), as described by Monin–Obukhov Similarity Theory (MOST), was used to investigate the presence of this delay. Theoretically, the Monin–Obukhov length scale (L) should include the effects associated with synoptic scale motion (Stull, 1988). L can be used as a scaling parameter to define the convective characteristics of the atmospheric boundary layer. Using this parameter, the effects of buoyancy and mechanical production of turbulence can be compared at a specific altitude. The surface layer scaling parameter ($-z/L$)

provides a metric indicating the strength of the convective conditions during the IOP period leading into the evening transition. We computed ϕ_h and $-z/L$ as follows:

$$\phi_h = \frac{kz}{\theta_{v*}^S L} \frac{\partial \theta_v}{\partial z} = \frac{kzu_*}{-w'\theta'_v} \frac{\partial \theta_v}{\partial z}, \quad (5)$$

$$-\frac{z}{L} = \frac{kzg(w'\theta'_v)_s}{\theta_{v*}^3}. \quad (6)$$

where k is the von Karman constant, z is the analysis altitude (2.23 m).

Figure 5 shows every 5 min ϕ_h as a function of $-z/L$ at 2.23 m for 30 June 2011 and 1 July 2011. Clearly, there are points which break away from MOST (indicated by the dashed black line). Specifically, gradient–theory fails locally due to the countergradient observations that appear in the plots during near stable conditions. Formally, MOST should be valid in the stable layer. However, during the transition period, one can observe that the log surface layer locally disappears close to the ground as there is a decoupling between the old log–layer and the newly forming stable layer, as shown in the transitioning temperature profile in Fig. 2. In the past, this phenomenon was mainly observed for the air–sea boundary layer (Sahlee et al., 2008). However, Smedman et al. (2007) also observed this behavior at a site over land, but for atmospheric conditions that were quite different from our study case. In particular, their case was for strong winds between $7\text{--}10 \text{ ms}^{-1}$ in contrast with BLLAST calm conditions.

4.2 Convective time analysis

To provide support for our delay hypothesis, the convective time scale is analyzed and compared to the delay time scale. The convective time scale can be defined as the approximate time that it takes one eddy to traverse the atmospheric boundary layer. The hypothesis described above should be supported, if the value of the delay and the value of the convective time are similar. In other words, the delay exists as a result of the continued movement of the boundary layer due to the last eddy motions generated at the surface.

It should be noted that there is debate in the research community regarding the use of various time scales during the transition period. There is not a general agreement about which scaling time is the best option during afternoon/evening transition (Nieuwstadt and Brost, 1986; Lothon et al., 2014). However, it will be used to learn more about the theory proposed.

First, the convective time scale (t_*) is computed following Deardorff (1972):

$$t_* = \frac{z_i}{w_*}, \quad \text{where } w_* = \left[\frac{gz_i}{\theta_v} \overline{w'\theta'_v} \right]^{\frac{1}{3}} \quad (7)$$

being z_i the boundary–layer depth. These scales are then computed averaging the 5 min periods just before the buoy-

365 ancy flux vanishes. The depth of the boundary layer was ob-
 370 tained from the BLLAST campaign's UHF profiler, which
 was installed approximately 150 m away from the 10 m
 tower. Specifically, we estimate the height of the ABL from
 the local maxima of the refractive index structure coefficient
 Lothon et al. (2014).

375 The results from the calculation of the convective time
 scale for all IOPs are shown in Table 1 and Fig. 6. It is clear
 that the delay time and the convective time compare better
 on some IOPs than others. For some IOPs, such as the 24
 June 2011 and the 30 June 2011, the delay time is nearly the
 same as the convective time. However, on other days, such
 as the 25 or the 27 June, the convective scale and delay time
 compare quite poorly.

380 These observed differences between the time scales could
 be a result of the characteristics of the boundary layer asso-
 ciated with the different IOPs that are not accounted for in
 the assumptions associated with the convective time scale.
 In other words, IOPs associated with very convective condi-
 tions seem to follow the theory better, while more synopti-
 cally forced conditions fail.

385 4.3 Monin–Obukhov length analysis

In contrast to subsection 4.1, here we computed a character-
 istic surface layer scaling parameter ($-z/L$) for each of the
 IOPs by averaging it over the time period prior to the main
 evening transition (from 1200 UTC to 1645 UTC). From the
 results, we observe that each IOP can be classified as a con-
 vective or weakly convective day (see Table 1). The most
 convective IOPs were 24 and 30 June 2011. These IOPs were
 also those with a better correlation between the delay time
 and the convective time scale (see Fig. 6 and Table 1). On the
 other hand, the weaker convective days (i.e., 25 and 27 June
 2011) show larger difference between the delay and convective
 times (see Table 1). Less convective days have higher
 values of u_* as a result of increased mechanical turbulence
 production close to the ground (2.23 m). On these weakly
 convective days, the delay time is increased as shear prevents
 the rapid onset of a stable boundary layer at the surface.

Figure 7 shows the difference between the two time scales
 as a function of $-z/L$. Evidently, the BLLAST data indicate
 an exponentially decreasing relationship between the time
 scale and the Monin–Obukhov parameter. This relationship
 is likely to be a function of local effects and should be inves-
 tigated at other sites to see if a general relationship can be
 ascertained. Regardless, Fig. 7 shows a potentially site spe-
 cific method for forecasting the delay time using midday data
 from a single flux tower.

440 4.4 Turbulent Rayleigh number analysis

The Turbulent Rayleigh number (Ra_{turb}) can be used to ex-
 plain the behavior of the delay time. It is calculated with Eq.
 1 but instead to use molecular thermal diffusivity (κ) and

molecular kinematic viscosity (ν), we use the turbulent ther-
 mal diffusivity (see Eq. 3) and turbulent viscosity (see Eq. 4).
 Therefore, Ra_{turb} reads:

$$Ra_{turb} = \frac{g}{\theta_v} \frac{\Delta\bar{\theta}_v(\Delta z)^3}{K_H K_M}, \quad (8)$$

where Δz is the distance between the sensors (8.2 – 2.23
 m). We select these two sensors because this area with an
 evolution closer to the idea proposed by Bénard. Turbulent
 thermal diffusivity and turbulent viscosity could play a role
 in the initiation or the ceasing of convection. We define the
 transitional turbulent Rayleigh number (Ra_t) as the value of
 Ra_{turb} when the buoyancy flux ceases. Figure 8 shows the
 temporal evolution of buoyancy flux and Ra_{turb} from 1700
 to 2000 UTC on 30 June and 1 July 2011. As can be ob-
 served, Ra_{turb} becomes negative later on 1 July 2011 simi-
 larly to the changes in sign of the local virtual potential tem-
 perature gradient. For all the analyzed days, BF is negative
 several tens of minutes before Ra_{turb} . Table 1 shows this
 temporal difference and the value of Ra_t . As can be ob-
 served, this temporal difference is clearly related with DT
 being larger the days with a larger temporal difference in be-
 tween Ra_t and BF .

We assume that, on each day, Ra_t is in correspondence
 with the critical Rayleigh number (Ra_{cr}). It is important to
 notice that during early morning, on those days with large
 values of Ra_{cr} larger values of buoyancy flux are needed to
 onset convection. Additionally, during the evening transition
 on these days, convection stops quickly when the buoyancy
 flux ceases. By assuming $Ra_t \propto Ra_{cr}$, larger values of Ra_t
 have to be observed on these days. Figure 9 shows $DT-t_*$
 as a function of Ra_t for all the studied days. There is an
 exponentially decreasing relationship between both paramet-
 ers. IOPs with larger Ra_t have a smaller difference between
 the convective and the delay time, meaning convection stops
 quickly. On the contrary, those days with low values of Ra_t ,
 their convection slowed down smoothly increasing the delay
 time and consequently $DT-t_*$.

5 Conclusions

It has been shown that there is a clear failure of flux gradient
 theory during the evening transition period as a result of non-
 local processes. Analysis of the data obtained from a 10-m
 tower during the BLLAST campaign indicates that a delay
 time exists between the time when the buoyancy flux ceases
 and the change in sign of the vertical gradient of the virtual
 potential temperature. This was the case for all IOPs.

For strong to moderate convective days, the delay time is
 relatively short (~ 30 – 40 min) and corresponds closely to the
 time scale associated with the last eddy movements. In other
 words, it is similar to the convective time scale. On the other
 hand, when midday convection is weaker, mechanical forces
 play a much larger role resulting in a larger friction velocity.

In these cases, the delay time is larger due to the increase of horizontal turbulence. The data support an exponential relationship between the difference in the delay time and the convective time scale and the Monin–Obukhov parameter $-z/L$.⁵²⁰ If found to be generalizable, this relationship could be used to help forecast the delay time using midday measurements (for days where large scale forcings are changing slowly).

Finally, we defined a transitional turbulent Rayleigh number (Ra_t) associated with the buoyancy flux cease. We observe that higher values of Ra_t are related with a faster decay of the convection. Otherwise, turbulent viscosity and thermal diffusivity help to slow down the last eddy movement and increase the delay time when we observe low values of Ra_t .⁵³⁰

In order to generalize the observations described in this paper, future work should investigate the delay hypothesis over additional convective days and various types of surfaces. To accomplish this, it is recommend that future observational campaigns include sufficient temperature and flux measurements near the ground to sufficiently resolve the countergradient processes.⁵³⁵

Acknowledgements. The authors wish to thank Dr. Andrey Grachev for his thoughts and advice on the topic presented and Jens Bange for his interesting comments during the revision process.⁵⁴⁰

This project was performed under the Spanish MINECO projects CGL2009–08609, CGL2012–37416–C04–03 and the European POCTEFA 720 FluxPyr program. The stage at the University of Utah was performed under the Spanish MINECO projects EEBB–I–12–05228. This work was partially supported by the United States Office of Naval Research, Award #N00014–11–1–0709.⁵⁴⁵

The BLLAST field experiment was made possible thanks to the contribution of several institutions and supports: INSU-CNRS (Institut National des Sciences de l’Univers, Centre National de la Recherche Scientifique, LEFE–IDAO program), Météo-France, Observatoire Midi–Pyrénées (University of Toulouse), EUFAR (European Facility for Airborne Research) and COST ES0802 (European Cooperation in the field of Scientific and Technical). The field experiment would not have occurred without the contribution of all participating European and American research groups, which all have contributed in a significant amount. BLLAST field experiment was hosted by the instrumented site of Centre de Recherches Atmosphériques, Lannemezan, France (Observatoire Midi–Pyrénées, Laboratoire d’Aérodologie). BLLAST data are managed by SEDOO, from Observatoire Midi–Pyrénées.⁵⁵⁰

References

- Angevine, W. M.: 2007, Transitional, entraining, cloudy, and coastal boundary layers, *Acta Geophys.*, **56**(1), 2–20.⁵⁷⁰
- Beare, R. J., J. M. Edwards, and A. J. Lapworth: 2006, Simulation of the observed evening transition and nocturnal boundary layers: large-eddy modelling. *Q. J. R. Meteorol. Soc.*, **132**, 61–80.
- Businger, J. A., J. C. Wyngaard, Y. Izumi, and E. F. Bradley, 1971: Flux-Profile Relationships in the Atmospheric Surface Layer. *J. Atmos. Sci.*, **28**, 181–189.
- Chapra, S. C. and Canale, R. P.: 1998, Numerical Methods for Engineers. Boston: McGraw-Hill Companies, 3 ed..
- Cole, G. S. and H. J. S. Fernando: 1998, Some aspects of the decay of convective turbulence. *Fluid. Dyn. Res.*, **23**(3), 161–176.
- Darbieu, C., F. Lohou, M. Lothon, F. Couvreux, D. Pino, P. Durand, E. Blay–Carreras and J. Vilà–Guerau de Arellano: 2014, Evolution of the turbulence during the afternoon transition of the convective boundary layer: a spectral analysis *J. 21st Symposium on Boundary Layer and Turbulence, 8-13 June 2014. Leeds (UK)*.
- Deardorff, J.: 1972, Numerical Investigation of Neutral and Unstable Planetary Boundary Layers. *J. Atmos. Sci.*, **7**(29), 91–115.
- Edwards, J. M., R. J. Beare, and A. J. Lapworth: 2006, Simulation of the observed evening transition and nocturnal boundary layers: Single-column modelling. *Q. J. R. Meteorol. Soc.*, **132**(614), 61–80.
- Fedorovich, E., F. T. M. Nieuwstadt, and R. Kaiser: 2001, Numerical and laboratory study of horizontally evolving convective boundary layer. Part II: Effects of elevated wind shear and surface roughness, *J. Atmos. Sci.*, **58**(6), 546–560.
- Franchitto, S. H. and V. B. Rao: 2003, The correlation between temperature gradient and eddy heat flux in the northern and southern hemispheres, *J. Meteorol. Soc. Japan. Ser. II*, **81**(1), 163–168.
- Ghan, S. J.: 1981, Modelling the synoptic scale relationship between eddy heat flux and the meridional temperature gradient.
- Grimsdell, A. W. and W. M. Angevine: 2002, Observations of the afternoon transition of the convective boundary layer, *J. Appl. Meteorol.*, **41**(1), 3–11.
- Haeffelin, M., F. Angelini, Y. Morille, G. Martucci, S. Frey, G.P. Gobbi, S. Lolli, C.D. O’Dowd, L. Sauvage, I. Xueref-Rémy, B. Wastine, and D.G. Feist: 2012, Evaluation of mixing-height retrievals from automatic profiling lidars and ceilometers in view of future integrated networks in europe, *Bound.–Lay. Meteorol.*, **143**(1), 49–75.
- Holtslag, A. A. M. and C. Moeng: 1991, ‘Eddy diffusivity and countergradient transport in the convective atmospheric boundary layer, *J. Atmos. Sci.*, **48**(14), 1690–1698.
- Holtslag, A. A. M. and C. Moeng: 1991, Local versus nonlocal boundary-layer diffusion in a global climate model, *J. Climate*, **6**, 1825–1842.
- Kundu P. J. and I. M. Cohen: 2010, *Fluid Mechanics*. Academic Press, Waltham (MA), USA, 904 pp.
- Lothon, M. and D. Lenschow: 2010, ‘Studying the afternoon transition of the planetary boundary layer, *Eos Trans. AGU*, **91**(29), 253–260.
- Lothon, M., Lohou, F., Pino, D., Couvreux, F., Pardyjak, E. R., Reuder, J., Vilà–Guerau de Arellano, Durand, P., Hartogensis, O., Legain, D., Augustin, P., Gioli, B., Faloona, I., Yagüe, C., Alexander, D., Angevine, W., Bargain, E., Barrié, J., Bazile, E., Bezombes, Y., Bezombes, Y., Blay–Carreras, E., van de Boer, A., Boichard, J. L., Bourdon, A., Butet, A., Campistron, B., de Coster, O., Cuxart, J., Dabas, A., Darbieu, C., Deboudt, K., Delbarre, H., Derrien, S., Flament, P., Fourmentin, M., Garai, A., Gibert, F., Graf, A., Groebner, J., Guichard, F., Jiménez M. A., Jonassen, A., von Kroonenberg, M., Lenschow, D., Magliulo, V., Martin, S., Martínez, D., Mastroiello, L., Moene, A., Molinos, F., Moulin, E., Pietersen, H., Pigué, B., Pique, E., Román-Gascón, C., Rufin–Soler, C., Saïd, F., Sastre–Marugán, M., Seity, Y., Steeneveld, G. J., Toscano, P., Traullé, O., Tzanos, D., Wacker, S., Wildmann, N., and Zaldei, A.: The BLLAST field

- experiment: Boundary–Layer Late Afternoon and Sunset Turbulence, *Atmos. Chem. Phys. Diss.*, 14, 10789–10852, 2014.
- Mahrt, L.: 1998, Nocturnal boundary–layer regimes, *Bound.–Lay. Meteorol.*, **88**(2), 255–278.
- 580 Moeng, C.-H. and P. P. Sullivan: 1994, A comparison of shear– and buoyancy–driven planetary boundary layer flows, *J. Atmos. Sci.*, **51**(7), 999–1022.
- Nadeau, D. F., E. R. Pardyjak, C. W. Higgins, H. J. S. Fernando, and M. B. Parlange: 2011, A simple model for the afternoon and
585 early evening decay of convective turbulence over different land surfaces, *Bound.–Lay. Meteorol.*, **141**(2), 301–324.
- Nieuwstadt, F. T. M.: 1984, The turbulent structure of the stable, nocturnal boundary layer, *J. Atmos. Sci.*, **41**(14), 2202–2216.
- Nieuwstadt, F. T. M. and R. A. Brost: 1986, The decay of convective
590 turbulence, *J. Atmos. Sci.*, **43**(6), 532–546.
- Pino, D., H. J. J. Jonker, J. Vilà–Guerau de Arellano, and A. Dossio: 2006, Role of shear and the inversion strength during sunset turbulence over land: Characteristic length scales, *Bound.–Lay. Meteorol.*, **121**(3), 537–556.
- 595 Pino, D., J. Vilà–Guerau de Arellano, and P. G. Duynkerke: 2003, The contribution of shear to the evolution of a convective boundary layer, *J. Atmos. Sci.*, **60**(16), 1913–1926.
- Sahlée, E., A. Smedman, A. Rutgersson U. Högström: 2007, Influence of a new turbulence regime on the global air–sea heat fluxes, *J. Climate*, **121**, 5925–5941.
- 600 Smedman, A., U. Högström, J.C.R. Hunt, and E.Sahlée: 2007, Heat/mass transfer in the slightly unstable atmospheric surface layer, *Q. J. R. Meteorol. Soc.*, **133**, 37–51.
- Sorbjan, Z.: 1996, Effects caused by varying the strength of the capping inversion based on a large eddy simulation model of the
605 shear–free convective boundary layer, *J. Atmos. Sci.*, **53**(14), 2015–2024.
- Sorbjan, Z.: 1997, ‘Decay of convective turbulence revisited’. *Bound.–Lay. Meteorol.*, **82**(3), 503–517.
- 610 Stull, R. B.: 1988, *An introduction to boundary layer meteorology*. D. Reidel Publ. Comp., Dordrecht, The Netherlands, 670 pp.
- Sullivan, P. P., C.-H. Moeng, B. Stevens, D. H. Lenschow, and S. D. Mayor: 1998, Structure of the entrainment zone capping the convective atmospheric boundary layer. *J. Atmos. Sci.*, **55**(19),
615 3042–3064.
- Van Dijk, A., Moene, A. F., and De Bruin, H. A. R.: 2004, The principles of surface flux physics: theory, practice and description of the ECPACK library. Internal Report 2004/1, Meteorology and Air Quality Group, Wageningen University, Wageningen, The Netherlands, 99 pp.
- 620 van Driel, Robert, H. J. J. Jonker: 2011, Convective Boundary Layers Driven by Nonstationary Surface Heat Fluxes *J. Atmos. Sci.*, **68**, 727–738.

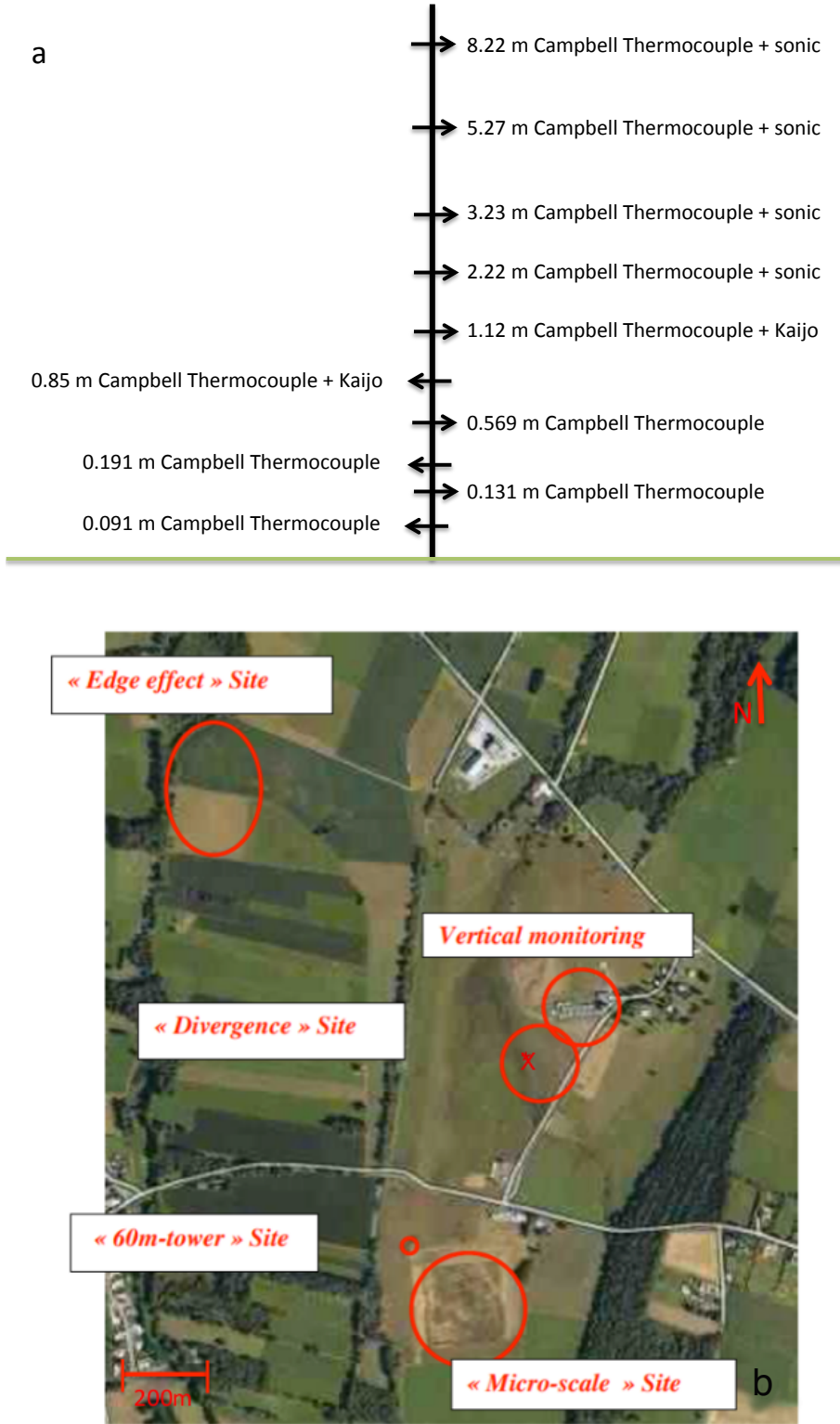


Fig. 1. (a) Sketch of the distribution of sensors that were deployed on the 10-m mast during BLLAST and (b) an aerial view of the site (the red X indicates the location of the 10-m tower).

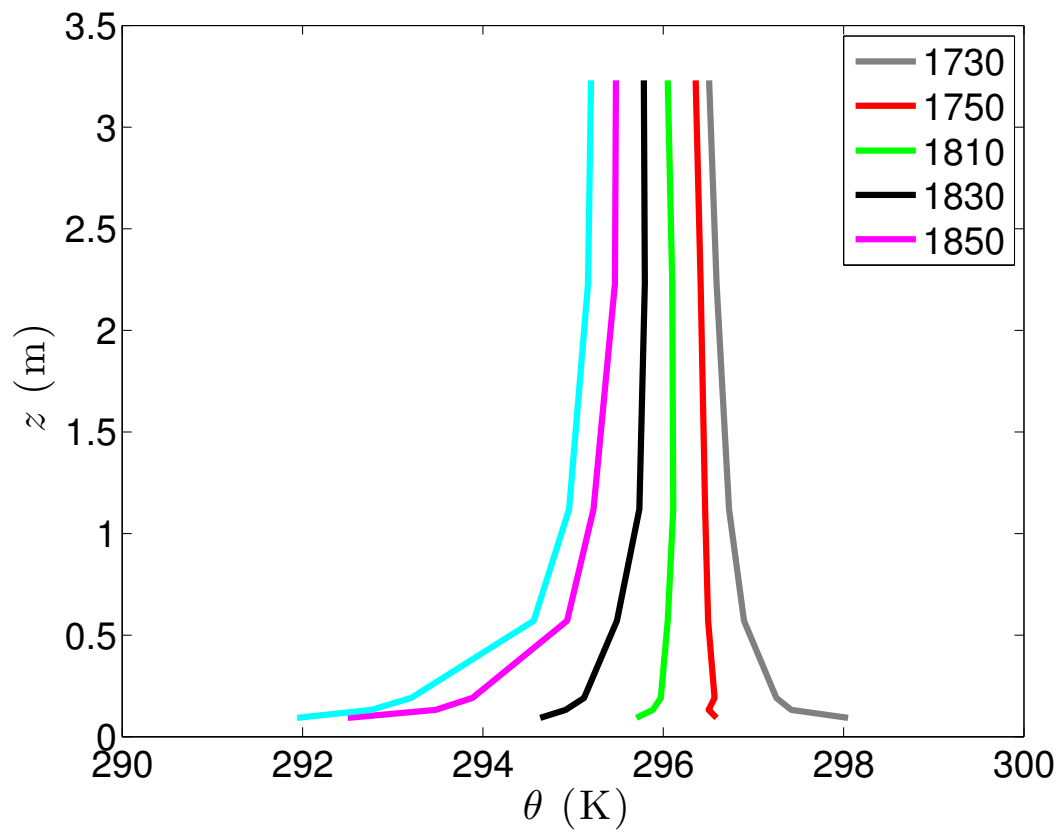


Fig. 2. Observed 5-min averaged vertical profile of potential temperature during the evening transition on 1 July 2011.

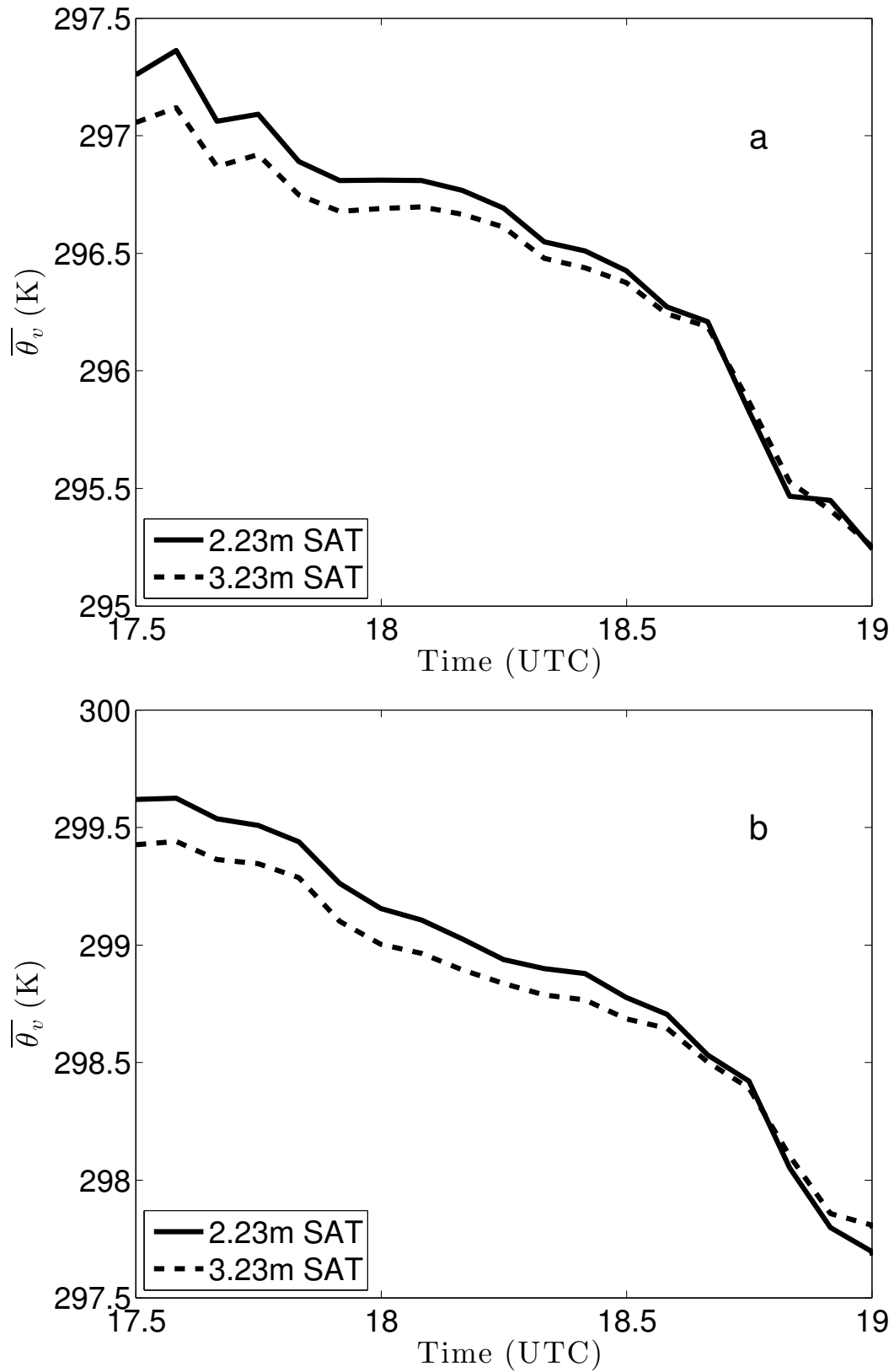


Fig. 3. Observed temporal evolution of the virtual potential temperature at 2.23 m (solid line) and 3.23 m (dashed line) during the evening transition on (a) 30 June and (b) 1 July 2011.

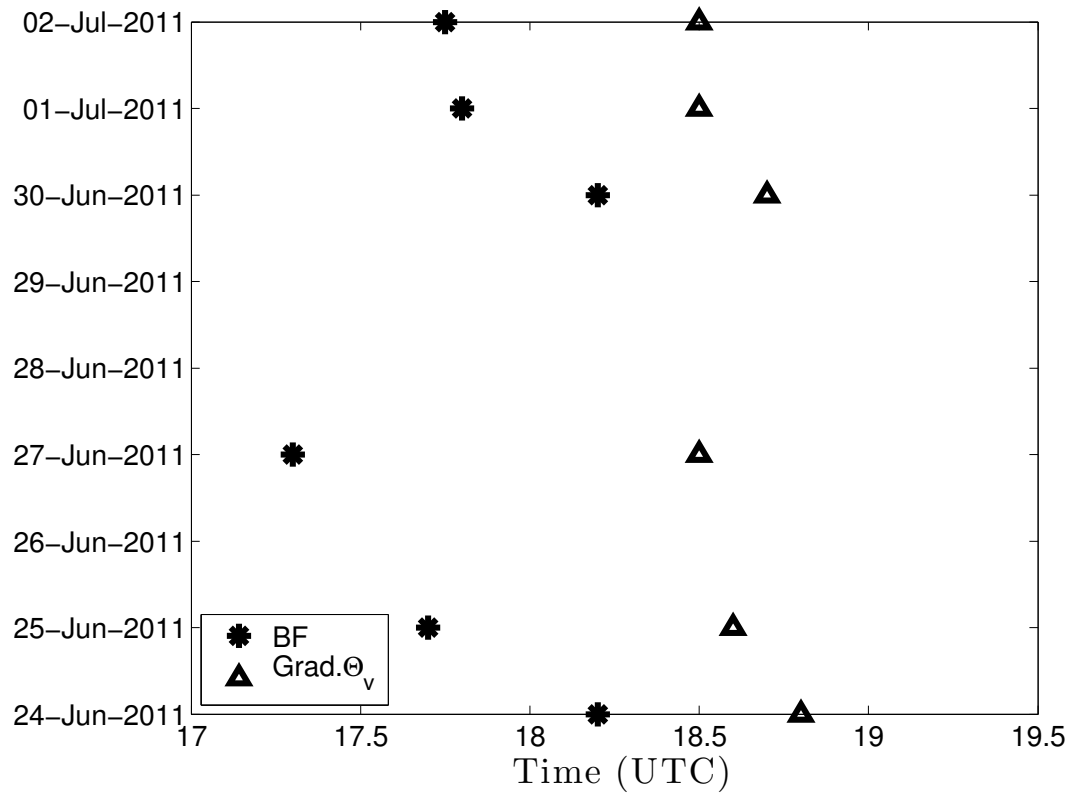


Fig. 4. For each IOP, instant when buoyancy flux (bullets) and virtual potential temperature gradient (triangles) change sign.

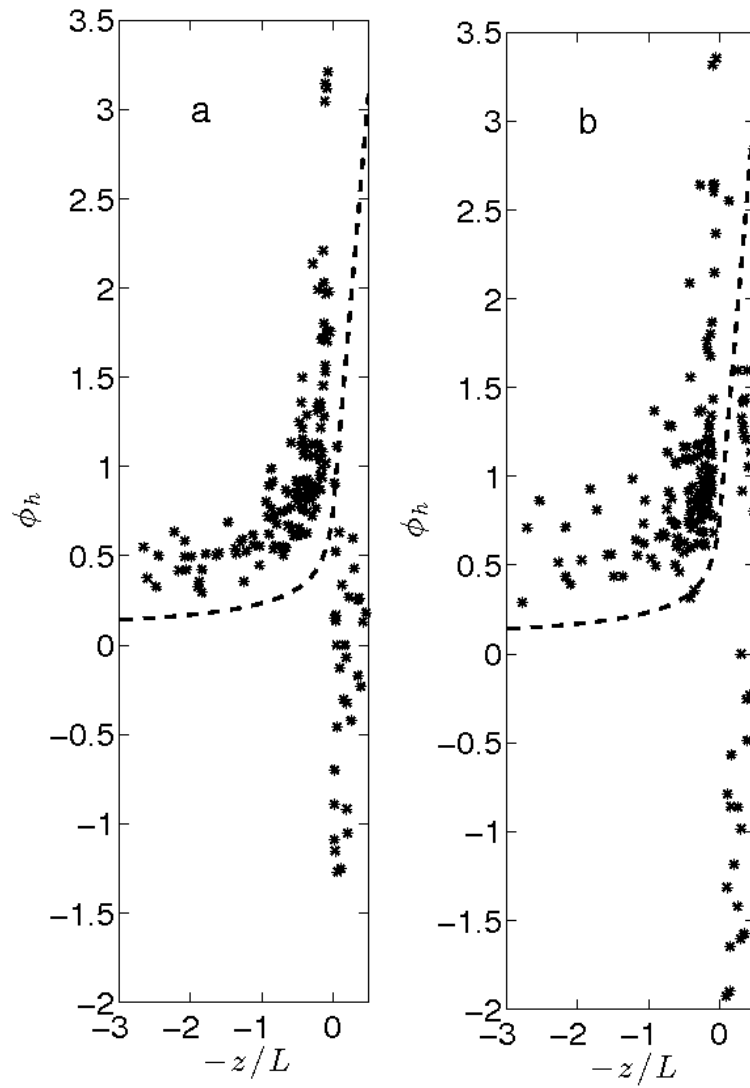


Fig. 5. Dimensionless temperature gradient (ϕ_h) as a function of $-z/L$ at 2.23 m on (a) 30 June and (b) 1 July 2011. Dashed line is the approximation of Businger et al. (1971)

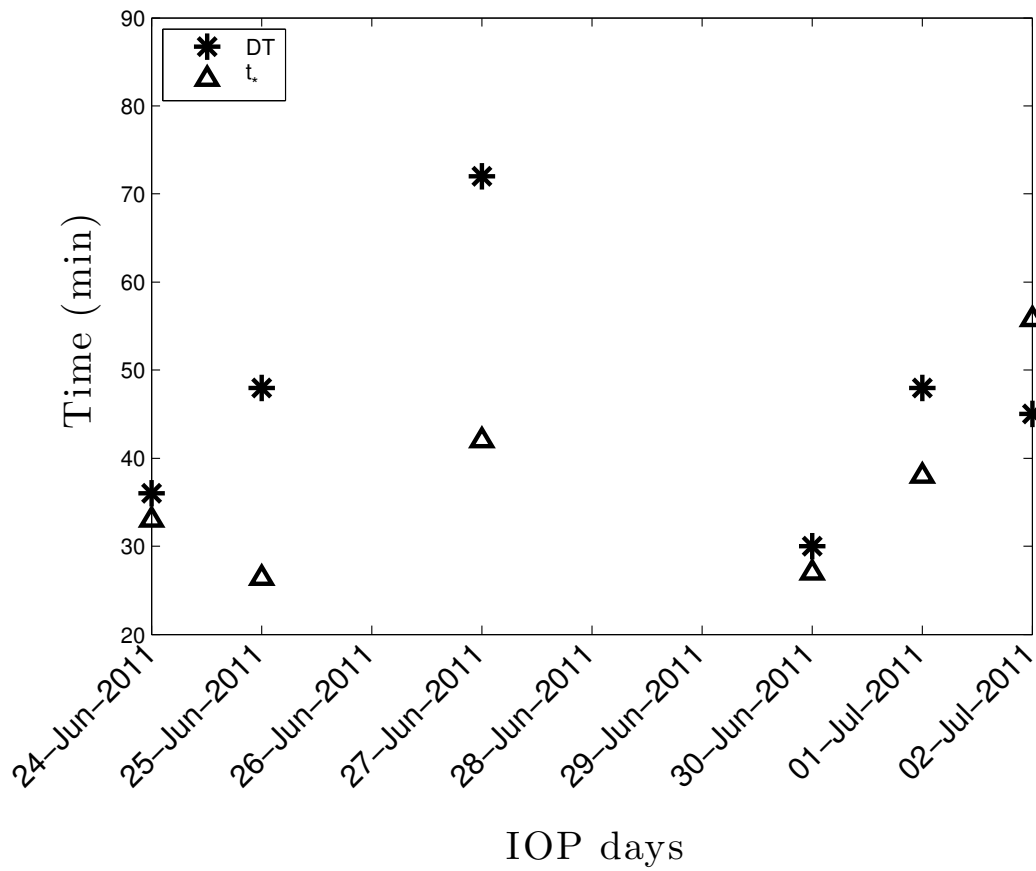


Fig. 6. For each IOP, delay (asterisks) and convective (triangles) times.

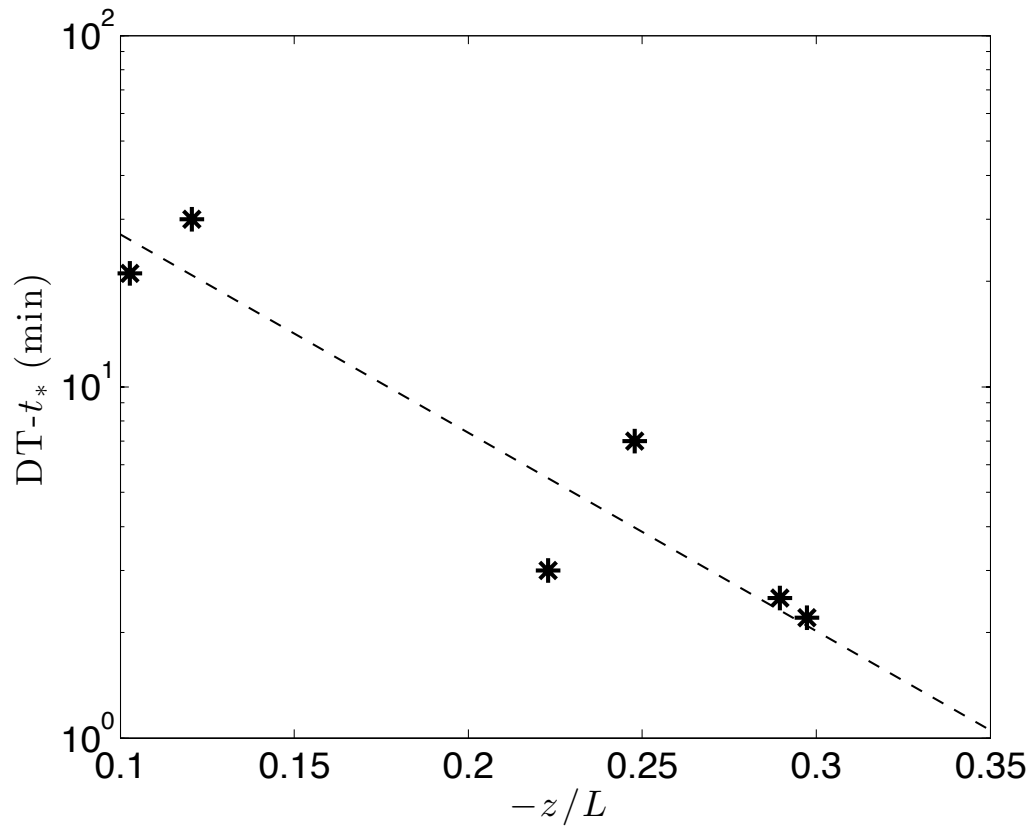


Fig. 7. For all the IOPs, difference between the delay and convective times as a function of $-z/L$.

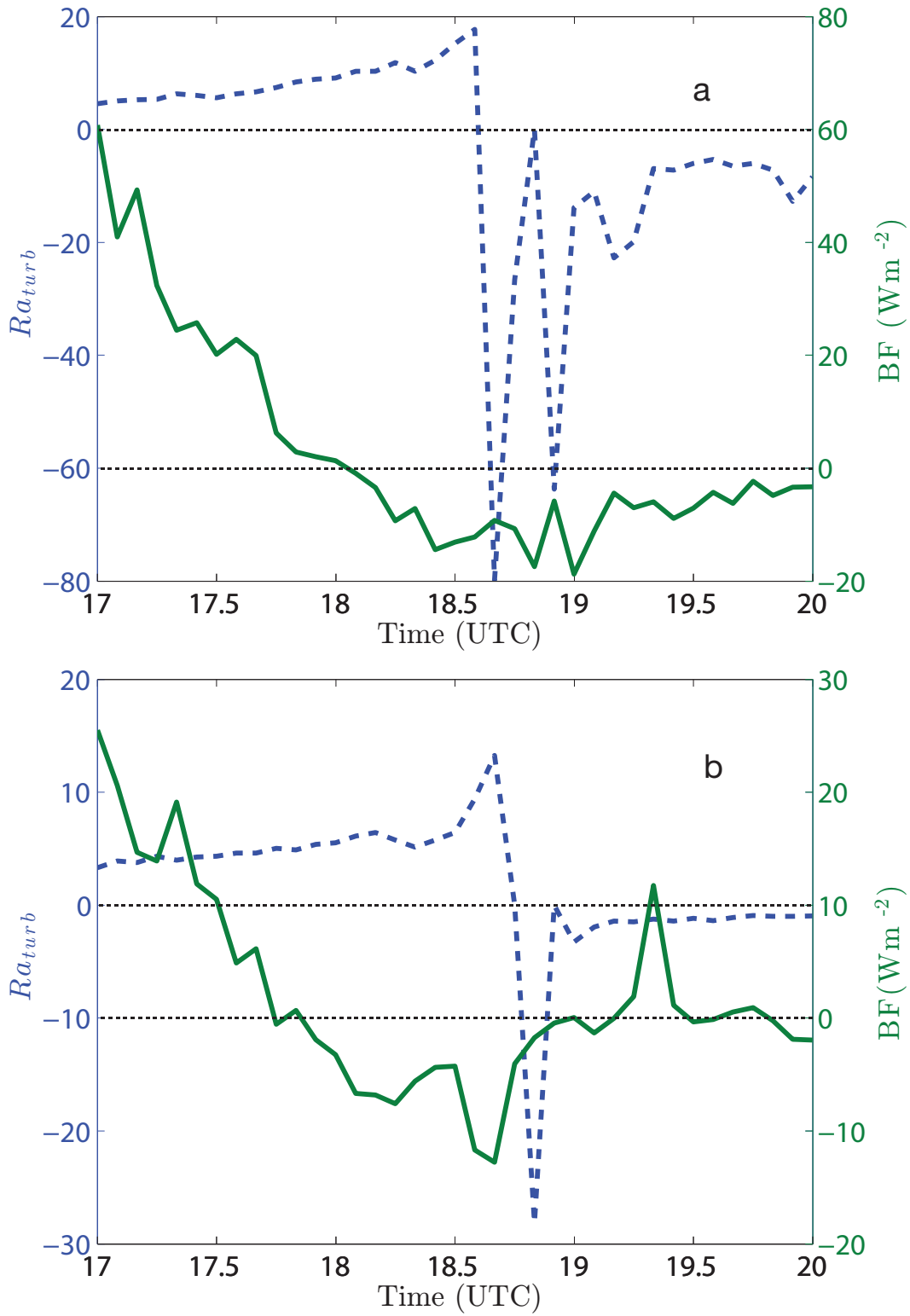


Fig. 8. Temporal evolution of buoyancy flux at 2.23 m (green) and Ra_{turb} (blue) during the evening on (a) 30 June and (b) 1 July 2011.

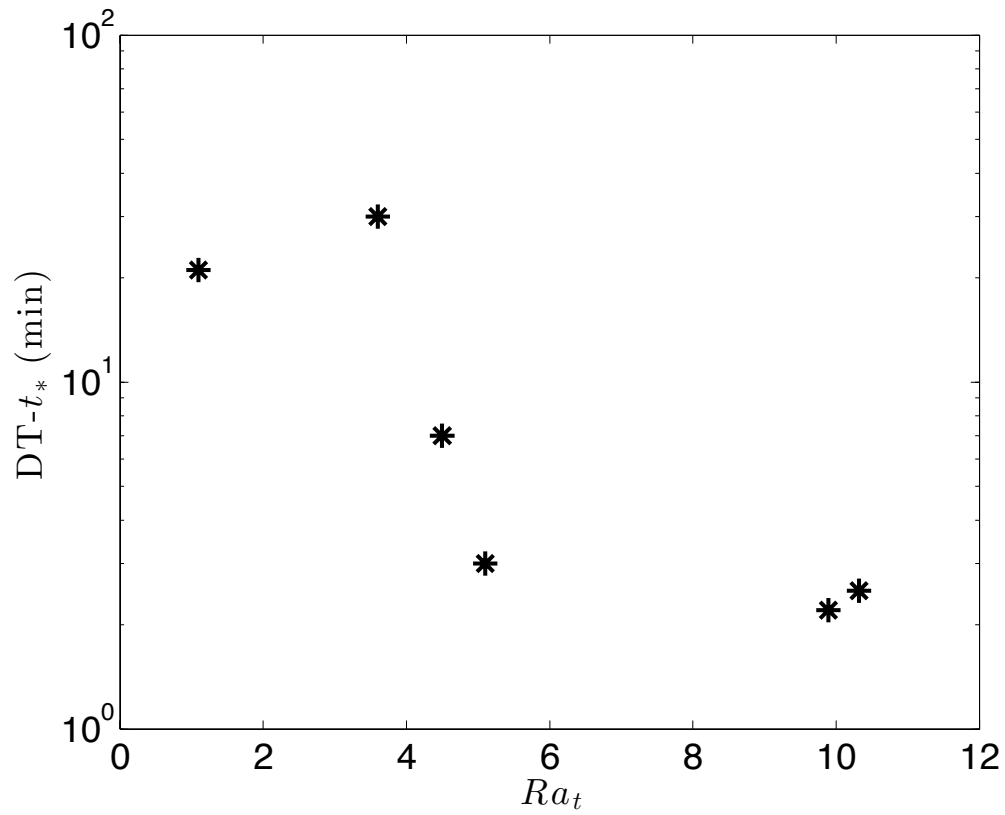


Fig. 9. For all the IOPs, difference between the delay and convective times as a function of transitional turbulent Rayleigh number (Ra_t).

Table 1. Based on the observations taken at BLLAST campaign, IOP day, maximum sensible heat flux, length of the day, days from last rainfall, delay time, convective time, convective intensity, transitional turbulent Rayleigh number and temporal difference between the time when Ra changes sign and buoyancy flux does it.

Day (IOP)	SH_{\max} (Wm^{-2})	Diurnal cycle (h)	Sunset (UTC)	Days from last rainfall	DT (min)	t_* (min)	$-z/L$	Convective definition	Ra_t	Ra_t-BF (min)
24 June (IOP4)	0.18	13.3	19:42	1	38	36	0.297	Convective	9.89	49
25 June (IOP5)	0.158	12.8	19:42	2	48	26.37	0.102	Weak	1.097	90
27 June (IOP7)	0.1	10.25	19:42	4	72	42	0.1205	Weak	3.62	95
30 June (IOP8)	0.11	12.16	19:42	1	30	27	0.289	Convective	10.32	34
1 July (IOP9)	0.138	12.8	19:41	2	40	33	0.22	Moderate	5.01	55
2 July (IOP10)	0.14	11.3	19:41	3	42	55.8	0.24	Moderate	4.5	53